An inverse Prandtl-Ishlinskii model based decoupling control methodology for a 3-DOF flexure-based mechanism

Z. Guo[1], Y. Tian[1], C. Liu[1], X. Liu[2], B. Shirinzadeh[3], F. Wang[1], D. Zhang[1]

[1]Key Laboratory of Mechanism Theory and Equipment Design of Ministry of Education, Tianjin University, Tianjin 300072, China

[2]School of Engineering, University of Warwick, Coventry CV4 7AL, UK

[3]Robotics and Mechatronics Research Laboratory, Department of Mechanical and Aerospace Engineering, Monash University, VIC 3800, Australia

Abstract： A modified Prandtl-Ishlinskii (P-I) hysteresis model is developed to form the feedforward controller for a 3-DOF flexure-based mechanism. To improve the control accuracy of the P-I hysteresis model, a hybrid structure that includes backlash operators, dead-zone operators and a cubic polynomial function is proposed. Both the rate-dependent hysteresis modeling and adaptive dead-zone thresholds selection method are investigated. System identification was used to obtain the parameters of the newly-developed hysteresis model. Closed-loop control was added to reduce the influence from external disturbances such as vibration and noise, leading to a combined feedforward/feedback control strategy. The cross-axis coupling motion of the 3-DOF flexure-based mechanism has been explored using the established controller. Accordingly, a decoupling feedforward/feedback controller is proposed and implemented to compensate the coupled motion of the moving platform. Experimental tests are reported to examine the tracking capability of the whole system and features of the controller. It is demonstrated that the proposed decoupling control methodology can distinctly reduce the coupling motion of the moving platform and thus improve the positioning accuracy and trajectory tracking capability.

Keywords: decoupling control, flexure-based mechanism, P-I hysteresis model, piezoelectric actuator.

1. Introduction

Micro/nano positioning is one of the key enabling techniques in the scientific and engineering fields including AFM (Atomic Force Microscopy) [1], STM (Scanning Tunnel Microscopy) [2], optical fiber alignment [3, 4], bio-micro-surgery [5, 6] and micro-assembly [7, 8]. In order to reach the required high precision, the piezo-driven flexure-based mechanism has been widely used due to the large output force and quick response [9-11]. However, the hysteresis of the piezoelectric ceramic significantly reduces the positioning accuracy of the developed system, so a variety of hysteresis models and control methodologies for the piezoelectric have been proposed. In addition, electromagnetic-driven flexure stage starts to be designed in recent years [12-14], especially in the requirement of large stroke, but electromagnetic drive such as voice coil motor usually owns small output force, leading to a small stiffness of the stage and further a low resonant frequency. In reference [15, 16], it is easy to find the mainstream modeling and control methods of piezo-actuated nanopositioning stages, and in reference [17], a corresponding general skeleton on this is presented. Among various hysteresis models such as Preisach model [18, 19], Bouc-Wen model [20, 21], Prandtl-Ishlinskii (P-I) model [22, 23], the P-I hysteresis model attracts more attention for the structural simplicity, easy model identification and analytical inverse. As a result, the P-I model is selected to model the hysteresis and further form a feedforward-feedback controller to control the motion of the platform.

Micro/nano planar positioning systems generally employ parallel kinematics mechanisms because of their compact structure, high stiffness and ease of monolithic fabrication [24, 25]. However, a degree of motion coupling between axes is one disadvantage for many potential applications. Although the coupling effects can be reduced to some extent through good mechanical design and optimization, the influences of assembly and manufacturing tolerances on the different axes will inevitably result in some residual coupling phenomena [26]. Further, the initial conditions of the installed piezoelectric actuators will significantly affect the static and dynamic properties, especially, the preload and the Hertzian contact between the piezoelectric actuator and the driving point. Discrepancy between the kinematic chains will induce motion coupling in such mechanisms, because the platform motion is determined by all of the kinematic chains in the parallel mechanism and apparently single-axis motion may depend on several actuators. For example, the rotational angle is implemented by driving three actuators simultaneously in the mechanisms described in [27, 28], two piezoelectric actuators are utilized to realize the rotational and translational displacement

in the mechanism described in [29]. Therefore, it remains important to develop a decoupling control methodology for parallel planar positioning systems even if their mechanism is designed with decoupling capability.

This paper proposes a modified inverse P-I hysteresis model, identified by a direct inverse modelling approach [30], to form the feedforward controller and thus compensate the nonlinearity of the piezoelectric actuators. In order to improve the accuracy of the hysteresis model without increasing the structural complexity, a hybrid structure of the inverse P-I hysteresis model is developed. It includes several serial connected backlash operators and dead-zone operators and a parallel connected cubic polynomial input function. A proportional-integral controller is added to form a feedforward/feedback controller to further improve the trajectory tracking performance of the developed flexure-based mechanism. A decoupling methodology has been proposed and constructed to reduce the coupling effects at the moving platform. The performance of the developed controller has been validated using a number of experimental tests. The rest of this paper is arranged as follows: Section II briefly describes the mechanical design and control system of the developed 3-DOF flexure-based mechanism. The modified P-I hysteresis model and parameter identification are provided in Section III. Section IV explores the decoupling feedforward/feedback control method for the 3-DOF flexure-based mechanism. Section V then examines the trajectory tracking capability of the developed controller. Finally, conclusions are drawn in Section VI.

2. 3-DOF flexure-based mechanism

A newly developed 3-DOF flexure-based micro/nano positioning mechanism is shown in Fig. 1(a). It is monolithically manufactured from an Aluminum Alloy T7075 plate using the Wire

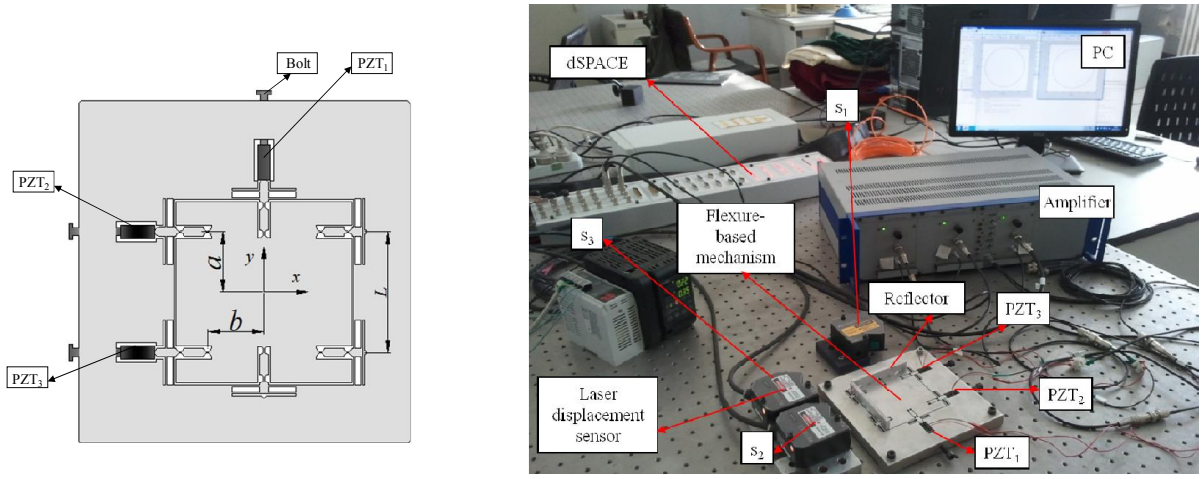

(a) 3-DOF flexure-based mechanism (b) Control system setup

Fig. 1. Developed 3-DOF flexure-based mechanism and control system.

Electric Discharge Machining (WEDM). The moving platform is supported by flexure-hinge links which are orthogonally arranged in the *x* and *y* directions. Two pairs of links are connected in parallel in the x direction and one pair of links in the *y* direction. Thus, the platform can translate in the *x* and *y* direction and rotate about the *z* axis. Three piezoelectric actuators are installed between the base and the driving points, and ball contacts (modeled as Hertzian) are used to avoid imposing bending force on the piezoelectric actuators (Model: AE 0505D18F, THORlabs Company USA). The preload is set by adjusting the bolt behind the actuator. The nominal maximal displacement of these specific actuators is 15 μm at the driving voltage of 100 V. After assemble the piezoelectric, the plane displacement of the flexure-based mechanism can reach 12.74 μm, 12.22 μm in the *x* and *y* direction, respectively, the maximal rotation angle in clockwise and anticlockwise are 0.0088° and 0.0103°, respectively, the first resonant frequency is 790 HZ in the θ_Z direction. More detailed information about the positioning mechanism can reference our previous work [31]. The actuators are driven by a piezoelectric amplifier (E-505.00, PI, Germany) that receives command signals from the I/O interface of a dSPACE DS1103 R&D control board, on which the newly developed control methodology is implemented with a sampling rate of 10 kHz. Three laser displacement sensors (LK-H050, Keyence, Japan) provide real time displacement sensing and measurement for the moving platform. Two of them are arranged in parallel in the *x* direction, allowing to translation in the *x* direction and rotation about the *z* axis be measured. The third one measures the platform displacement in the *y* direction. In order to reduce the influences of external disturbances, the whole system is mounted on a Newport RS-4000 optical table, as shown in Fig. 1(b).

3. The feedforward/feedback controller based on a modified inverse P-I hysteresis model

A new design of feedforward/feedback controller for the flexure-based mechanism, accounting for hysteresis and external disturbances, has been established and implemented in the dSPACE DS1103 R&D control board. The rate dependent hysteresis of the piezoelectric actuator is compensated by exploiting a modified inverse P-I hysteresis model in a feedforward controller, using the direct parameter identification technique. Then a closed-loop feedback controller is used to eliminate the effects of external disturbances such as vibration and noise on the positioning accuracy of the mechanism.

3.1. The modified inverse P-I hysteresis model

The traditional P-I hysteresis model is generally constructed from parallel-connected backlash operators which can be expressed as

$$H_r[u](t) = \max\left\{u(t) - r, \min\left\{u(t) + r, H_r[u](t - T)\right\}\right\}$$
$$H_r[u](0) = \max\left\{u(0) - r, \min\left\{u(0) + r, 0\right\}\right\} \quad (1)$$

where $H_r[u](t)$ is the output of the backlash operator, $u(t)$ is the input function, r is the threshold of backlash operator, and T is the sampling period. The start state of the backlash operator is determined by the initial energy condition of the actuation devices. If the actuator starts from the de-energized state, the initial condition can be set to zero.

Superposing several weighted backlash operators can effectively model the hysteresis loops with acceptable accuracy. However, the backlash operator has symmetrical shape about the central line and so the modeled hysteresis loop must also possess symmetrical characteristics. It is not a feasible model for applications in which the hysteresis loops show asymmetry and saturation properties. Thus, it is necessary to introduce a dead-zone operator [26] or a cubic polynomial input function [28, 29] to compensate such kinds of nonlinearity. The basic dead-zone operator is

$$S_d[u](t) = \begin{cases} \max\{u(t) - d, 0\}, & d > 0 \\ u(t) & d = 0 \end{cases} \quad (2)$$

where $S_d[u](t)$ is the output and d is the threshold of the dead-zone operator.

The standard literature notes that the saturation and asymmetry characteristics can be well modeled by multiple dead-zone operators. However, a number of parameters of the dead-zone operators need to be identified. Improving the modeling accuracy requires increasing numbers of the dead-zone operators, and thus results in the system complexity. To overcome this problem, a cubic polynomial function of the input trajectory is used to compensate the saturation and asymmetric properties of the hysteresis loops. The common configuration is to connect the dead-zone operators or cubic polynomial input functions in series with the backlash operators. In order to improve model accuracy without losing structural simplicity, a novel hysteresis model configuration is proposed. In this hysteresis model, the superposition of the weighted backlash operators is serially connected with the superposition of the weighted dead-zone operators, and then this whole sub-system is parallel connected with a cubic polynomial input function. Adopting the parallel connected cubic polynomial function can significantly reduce the need for dead-zone operators, leading to a simpler system with fewer parameters. Based on this proposal, the inverse P-I hysteresis model is established and shown in Fig. 2. The governing equation of the inverse hysteresis model is

$$u(t)=\Gamma^{-1}(y,\dot{y})=G(y)+\boldsymbol{w_h}^T\boldsymbol{H_r}\left[\boldsymbol{w_s}(\dot{y})^T\cdot\boldsymbol{S_d}[y](t)\right] \tag{3}$$

where $\boldsymbol{H_r}[u_1(t)]=[H_{r1}[u_1](t),\ H_{r2}[u_1](t),\ldots,\ H_{rn}[u_1](t)]^{\mathrm{T}}$ and $\boldsymbol{S_d}[y](t)=[S_{d1}[y](t),\ S_{d2}[y](t),\ \ldots,\ S_{dm}[y](t)]^{\mathrm{T}}$ are backlash operator vector and dead-zone operator vector, respectively, $w_h{}^{\mathrm{T}}=[w_{h1},\ w_{h2},\ w_{h3},\ \ldots,\ w_{hn}]^{\mathrm{T}}$ and $w_s{}^{\mathrm{T}}=[w_{s1},\ w_{s2},\ w_{s3},\ \ldots,\ w_{sm}]^{\mathrm{T}}$ are the backlash operator and dead-zone operator weightings, respectively, $G(y)=a_1y(t)^3+a_2y(t)^2+a_3y(t)+a_4$ is a cubic polynomial input function, y is the desired trajectory, and $u(t)$ is the output of the model.

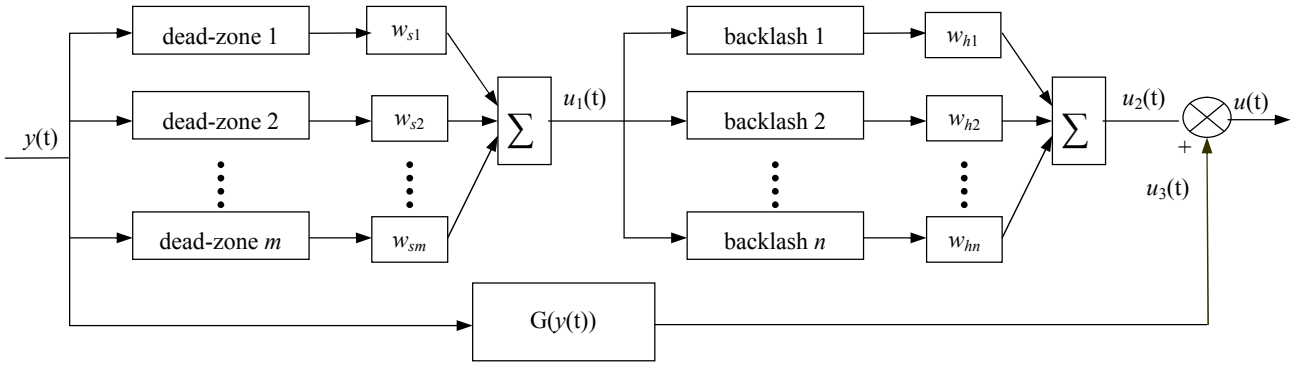

Fig. 2. Block diagram of modified inverse P-I hysteresis model.

The rate-dependence of the hysteresis loop is modeled in a simple but effective method, where the weights of the backlash operators change linearly with the input rate [26]. The linear relationship between the weight and the input rate is

$$\boldsymbol{w_h}=\boldsymbol{k}\dot{y}(t)+\boldsymbol{b} \tag{4}$$

where $\boldsymbol{k}=[k_1,\ k_2,\cdots,\ k_n]^{\mathrm{T}}$ and $\boldsymbol{b}=[b_1,\ b_2,\cdots,\ b_n]^{\mathrm{T}}$ are the slop and intercept vectors, respectively, which can be determined in the parameter identification.

The thresholds d and r are generally taken as constants in previous research [28, 29]. And the values of the thresholds are commonly chosen based on the personal experience, leading to uncertainty that significantly affects the modeling results. Thus, here, a variable c is introduced to adjust the values of these thresholds, which can be determined through experimental system identification. The parameter c directly optimizes the dead-zone threshold value d and further affects the backlash threshold value r, since the two components are cascaded, with the output of the dead-zone operators being the input of the backlash operators. When the maximal output of the dead-zone operators is smaller than some threshold values of backlash operators, these backlash operators will lose function, so an overall scale coefficient $u_{1\max}/10$ is applied to the backlash thresholds to guarantee that the entire set of backlash operators can operate effectively. The current implementation of the proposed inverse P-I hysteresis model uses ten backlash operators and six

dead-zone operators with a cubic polynomial input function. The thresholds of the dead-zone and backlash operators are

$$\begin{cases} \boldsymbol{d} = c\left[0, 1, 3, 5, 7, 9\right]^{\mathrm{T}} \\ \boldsymbol{r} = \left[0, 0.25, 0.5, 1, 1.5, 2.25, 3, 4, 5, 6.5\right]^{\mathrm{T}} u_{1\max} / 10 \end{cases} \tag{5}$$

The least square curve fitting method was adopted to conduct the parameter identification using the Matlab® software package. Three sinusoidal signals with frequencies of 1 Hz, 0.7 Hz, and 0.2 Hz are superimposed to generate the input command

$$u = 5.5 + 3\sin(2\pi t - 0.5\pi) + \sin(1.4\pi t - 0.5\pi) + 1.5\sin(0.4\pi t - 0.5\pi) \tag{6}$$

The objective function is defined as

$$F = \left\| u(t) - u \right\|_2^2 \tag{7}$$

where $u(t)$ is the output voltage of the proposed inverse hysteresis model and u is the actual input voltage.

Parameter identification must be undertaken for each of the three piezoelectric actuators used in the 3-DOF flexure-based mechanism. Parameter identification in the y direction is straightforward, since there is only one actuator in this axis. However, two parallel actuators (PZT_2 and PZT_3) are installed in the x direction. In order to obtain similar static and dynamic characteristics from them, the preloads on these two piezoelectric actuators were carefully adjusted until their maximum displacements were almost equal. By minimizing the error between the measured and desired data, the cubic polynomial input function were identified as

$$G(x(t)) = 0.119\times10^{-4}x^3 - 2.518\times10^{-2}x^2 + 1.005x - 0.272 \tag{8}$$

$$G(y(t)) = -6.587\times10^{-4}y^3 + 2.391\times10^{-2}y^2 + 0.628y - 0.380 \tag{9}$$

The parameter c was identified as 1.033 and 0.716 in the x and y directions, respectively, and the parameters of the backlash operators and dead-zone operators in the x and y directions are listed in Table 1. Fig. 3 shows the voltage applied to identify the model and compares the measured curve with the prediction. The good agreement indicates the correctness of the proposed inverse hysteresis model.

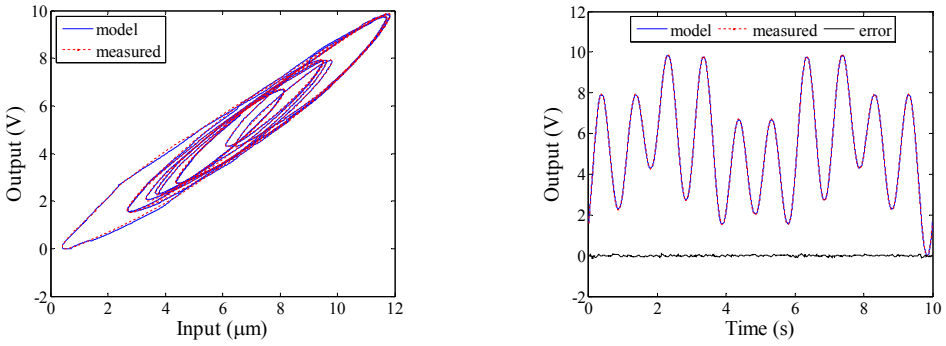

(a) (b)

Fig. 3. Identification results of inverse modified P-I model in the *y* direction: (a) inverse hysteresis loop of model and actual output; (b) time plot of model and actual output.

Table 1. Identified parameters in the *x* and *y* directions

	x			*y*		
i	$k_i(10^{-2})$	b_i	$w_{si}(10^{-2})$	$k_i(10^{-3})$	b_i	w_{si}
1	24.582	-1.415	-1.351	-6.585	1.191	-3.001
2	-26.332	1.549	5.660	9.993	-0.653	-2.737
3	2.409	0.856	2.915	0.784	-0.358	9.210×10^{-2}
4	-0.590	0.638	-2.259	-2.679	-7.630×10^{-2}	3.230×10^{-2}
5	-4.738	2.114	-1.095	1.071	-0.181	0.129
6	1.034	2.087	0.389	-2.371	-3.551×10^{-2}	-0.203
7	-3.011	1.403	/	34.135	0.263	/
8	20.546	-0.061	/	-112.860	2.675	/
9	-44.572	3.543	/	128.310	-4.102	/
10	-25.857	-3.441	/	-47.858	1.139	/

In order to show the advantages of the modified inverse P-I model, the paper focused on the comparison in the modeling accuracy and the response time. Two traditional inverse P-I models are selected for the comparison, the first one has ten backlash operators and six dead-zone operators, the second one has ten backlash operators and ten dead-zone operators, note that the latter model has same number of parameters with the proposed model.

The value of *F* in Eq. (7) is ideal to evaluate the modeling accuracy, in order to minimize the effects of accidents, thirty groups of random data are selected as the initial values of the three inverse P-I models and the minimal objective function value reflects the modeling accuracy. Through the simulation, the function value of the proposed inverse P-I model, the traditional inverse P-I model with ten and six dead-zone operators are 21.44, 30.09, 35.33, respectively, which indicates the proposed inverse P-I model has the highest modeling accuracy. In the comparison of the response time, the results of thirty times measurements are implemented and shown in Fig. 4,

which manifests both the proposed model and the model with ten dead-zone operators spend a longer response time, but the latter consume much more.

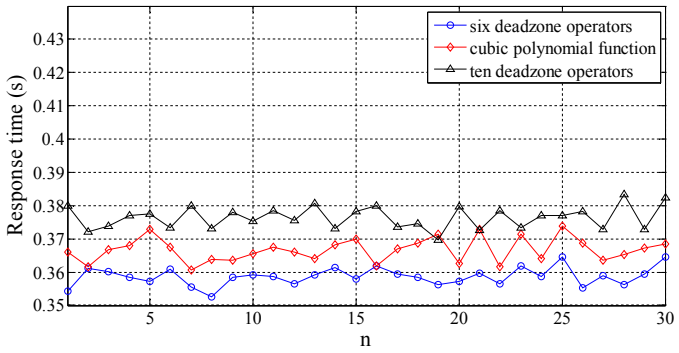

Fig. 4. Response time of three different inverse hysteresis models.

It is demonstrated that both the dead-zone operator and polynomial input function can be used to describe the asymmetric hysteresis [32]. However, the modelling precision with only polynomial input function is hardly further improved, and the modelling precision can be improved by increasing the number of the dead-zone operators resulting in an obvious increase of the response time. Thus, the combination of the dead-zone operator and polynomial input function overcame these problems effectively.

3.2. The feedforward/feedback controller

The modified inverse P-I hysteresis model can be used to form the feedforward controller, but it cannot compensate the unmodeled errors, including creep of the piezoelectric actuator and external disturbances such as vibration and noise, which also influence the positioning accuracy of the mechanism. These errors can be effectively compensated by feedback methods, so in order to improve the static and dynamic performance of the entire system, a combined feedforward/feedback controller is introduced. The feedback path uses a traditional Proportional Integral (PI) control algorithm, and the block diagram of the feedforward/feedback controller is shown in Fig. 5, y_d and y denote the desired and actual displacement of the flexure-based mechanism, respectively. Combined with the feedback control, the input voltage of piezoelectric actuator should be

$$u_{in} = \Gamma^{-1}\left(y_d, \dot{y}_d\right) + \left(k_p e(t) + k_i \int_0^t e(\tau) d_\tau\right) \tag{10}$$

where k_p and k_i are the proportional and integral gains of the feedback controller, respectively, e is the tracking error between desired and actual displacement, and $e = y_d - y$.

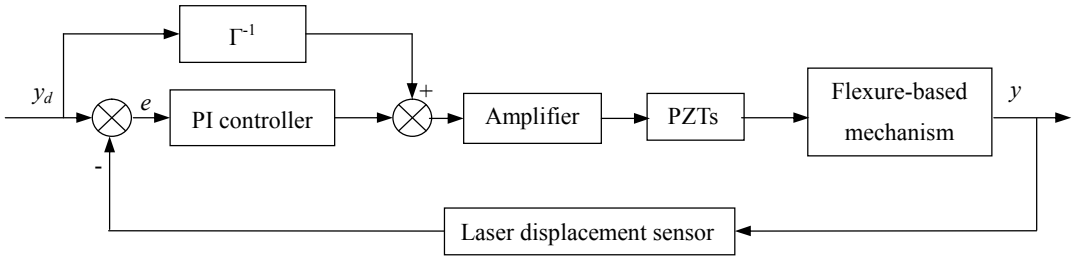

Fig. 5. Block diagram of feedforwar/feedback controller in the *y* direction.

The parameter of the feedback controller are tuned by the Ziegler-Nichols method, in translational direction k_p and k_i are 0.05 and 50, respectively, while in the motion rotate about the *z* axis they are 0.06 and 70, respectively.

There is only one piezoelectric actuator (PZT_1) in the *y* direction of the flexure-based mechanism, so the desired trajectory is transformed directly into the driving voltage of the piezoelectric actuator by combining the output of the modified inverse P-I hysteresis model with the compensation voltage, which is calculated by the Proportional Integral controller from the tracking error. The driving voltage is amplified by a piezoelectric amplifier with a gain of 10 before it is supplied to the actuator.

Realizing the motion in the *x* and θ_Z directions requires driving the other two piezoelectric actuators (PZT_2 and PZT_3). Expanding both of them simultaneously results in translational displacement of the platform in the *x* direction, while supplying command signals with the opposite and equal magnitude to the two actuators can generate the rotational motion about the *z* axis. Because the piezoelectric actuators cannot retract from their initial position (zero control voltage), so in order to implement the rotational motion of the platform, the home position in the *x* direction should be defined at the half stroke of the platform motion.

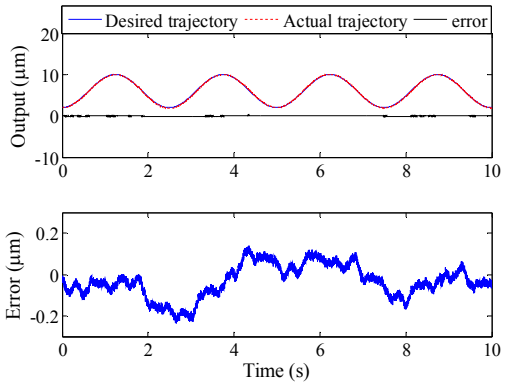

Fig. 6. The trajectory tracking of a sinusoidal signal in the *y* direction with feedforward controller.

The performance of the 3-DOF flexure-based mechanism with the newly-developed feedforward/feedback controller has been examined through sinusoidal signal tracking. In turn, the motion axis was driven (10 μm or 9.2×10-3 deg), with the demand on the other two axes held at zero. The displacements in driven and another two non-driven directions were recorded simultaneously by three laser displacement sensors. Note that x_2 and x_3 are parallel displacements measured by two sensors (s_2 and s_3 in Fig. 1(b)), they are used to calculate the output and coupling error in both the x and θ_Z axes.

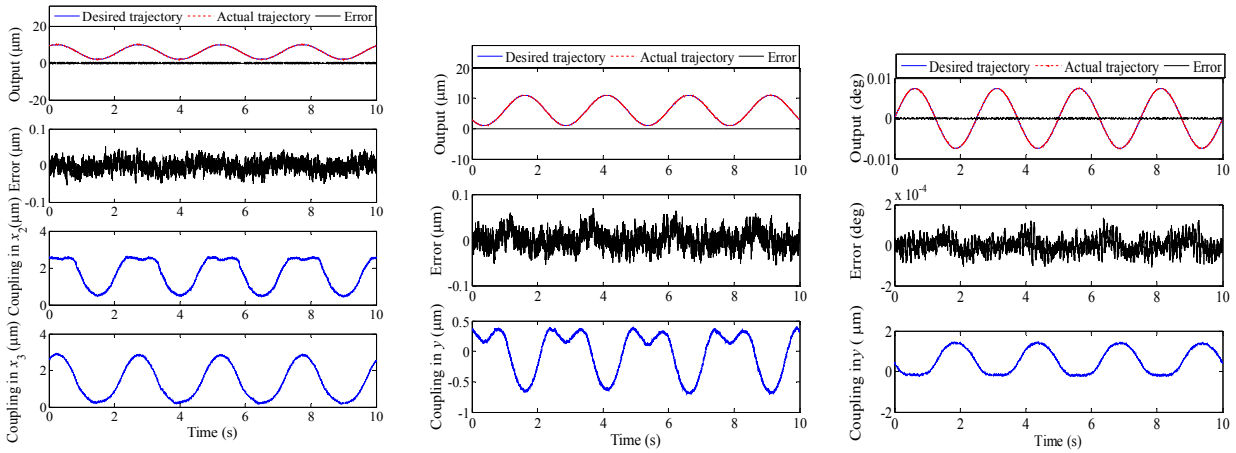

(a) (b) (c)

Fig. 7. The trajectory tracking of a sinusoidal signal and coupling error with feedforward/feedback controller: (a) trajectory tracking in the y direction and coupling error in x_2 and x_3; (b) trajectory tracking in the x direction and coupling error in y; (c) trajectory tracking in the θ_Z direction and coupling error in y.

As shown in Fig. 6, a sinusoidal signal in the y direction is tracked using feedforward controller, the maximal tracking error and root mean square (RMS) tracking error are 0.2389 μm and 0.0850 μm, respectively, which are used to compare the tracking property with the feedforward/feedback controller. Fig. 7 shows the experimental results for all three axes using feedforward/ feedback controller, and Fig. 7(a) is the tracking result in the y direction, the maximal tracking error and root mean square (RMS) tracking error are 0.0544 μm and 0.0134 μm, respectively, indicating that the feedforward/feedback controller is more effective than the feedforward controller in signal tracking. However, the coupling errors detected by s_2 and s_3 are too large to be neglected, at around 2 μm. It is obvious that the two measured coupling error are different, which might be caused by different initial conditions of the x-direction PZTs or possible assembly errors at the reflector, but is most likely a coupled rotation of the moving platform. Figs. 7(b) and (c) respectively show the maximal and RMS tracking errors, 0.0701 μm and 0.0171 μm in

the x direction and 1.21×10-4 deg and 3.3×10-5 deg in the θ_Z direction. Again, the cross-coupling displacement in the y direction is seriously large. Thus, it is essential to implement decoupling control to achieve precision capability for the planar trajectory tracking.

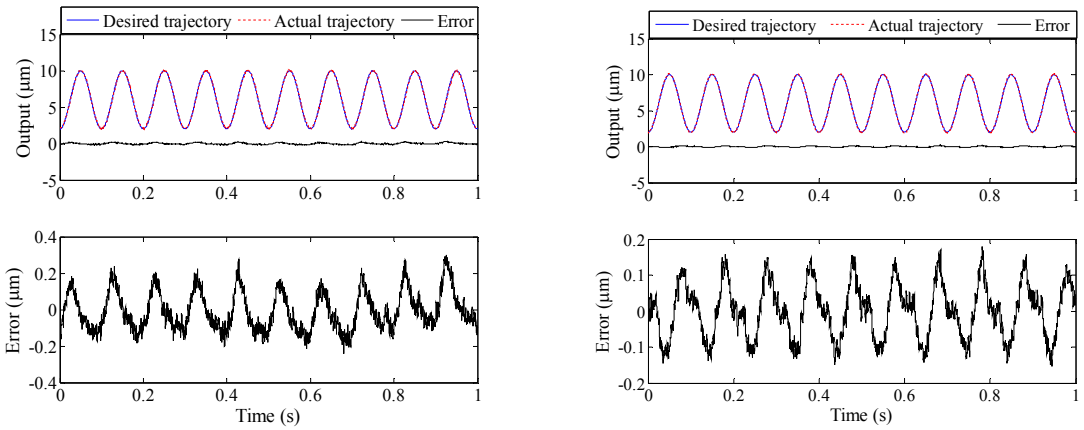

(a) Feedforward controller (b) Feedforward/feedback controller

Fig. 8. The trajectory tracking of a sinusoidal input in the y direction with a higher frequency.

What's more, in order to understand the bandwidth of the inverse P-I model based feedforward controller and the corresponding feedforward/feedback controller, a higher frequency input signal with 10 HZ is tracked and the results are shown in Fig. 8, indicating both the controller are effective in tracking higher frequency signal, and obviously the feedforward/feedback controller has a better tracking property.

4. The decoupling Feedforward/feedback controller

Even if ideally designed in principle, a real 3-DOF flexure-based mechanism will exhibit some coupling motions between different motion directions because of inevitable manufacturing and assembly errors. Although the mechanism used here is monolithically fabricated with a symmetric structure, there will be machining errors from the WEDM process. Also, the installation of the piezoelectric actuators will introduce additional stiffness in that side of the moving platform and thus disturb the symmetric properties of the entire system. However, when the platform is actuated, any coupled error motions will degrade its tracking property of a 2-D trajectory, so a decoupling strategy has been introduced as a necessary part of the controller.

The coupling errors can be compensated by adjusting the input voltages of the piezoelectric actuators in the coupled directions. This can be realized in practice by changing the input signal to the modified inverse P-I hysteresis model, and this signal can be achieved by adding the decoupling control algorithm onto the previous version of the controller. Fig. 9 shows the block diagram of the decoupling feedforward /feedback controller. The decoupling compensation signal for the non-actuated directions is calculated based on the experimental results from single axis actuation testing (Fig.7), and these signals are just compensated to the input command of the modified inverse P-I model, the tracking error *e* still determined by difference between the desired displacement and the measured displacement.

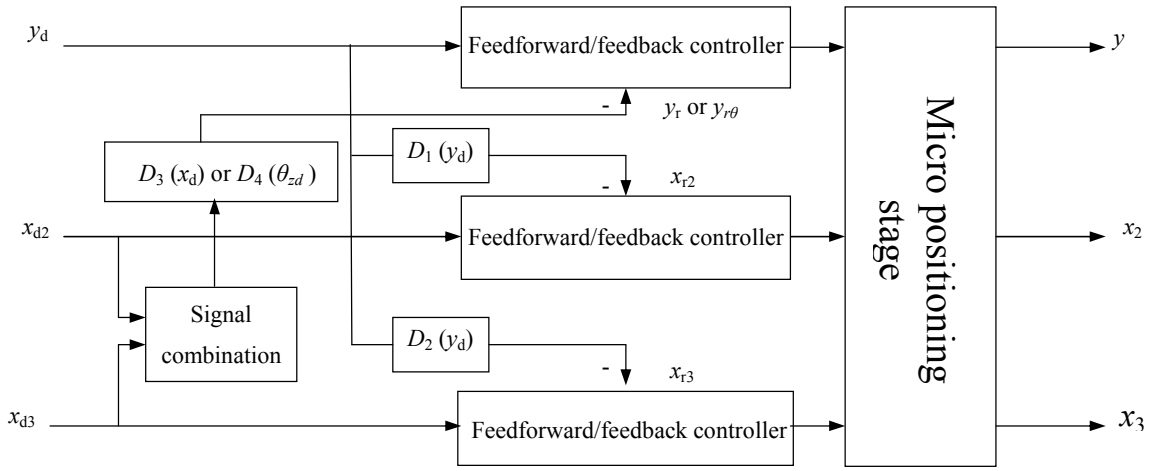

Fig. 9. Block diagram of decoupling feedforward/feedback controller.

The decoupling algorithm is defined as

$$\begin{bmatrix} x_{r2} \\ x_{r3} \\ y_{rx} \\ y_{r\theta} \end{bmatrix} = \begin{bmatrix} x_{d2} \\ x_{d3} \\ y_d \\ y_d \end{bmatrix} + \begin{bmatrix} D_1\left(f_1\left(y_d\right)\right) \\ D_2\left(f_2\left(y_d\right)\right) \\ D_3\left(f_3\left(x_d\right)\right) \\ D_4\left(f_4\left(\theta_{zd}\right)\right) \end{bmatrix} = \begin{bmatrix} x_{d2} \\ x_{d3} \\ y_d \\ y_d \end{bmatrix} + \begin{bmatrix} D_1\left(\Delta k_1 y_d + \Delta b_1\right) \\ D_2\left(\Delta k_2 y_d + \Delta b_2\right) \\ D_3\left(\Delta k_3 x_d + \Delta b_3\right) \\ D_4\left(\Delta k_4 \theta_{zd} + \Delta b_4\right) \end{bmatrix} \tag{11}$$

where $\begin{bmatrix} x_d \\ \theta_{zd} \end{bmatrix} = \begin{bmatrix} \left(x_{d2} + x_{d3}\right)/2 \\ \left(x_{d2} - x_{d3}\right)/L \end{bmatrix}$, $D_i\left(f_i\right) = \begin{cases} p_i & f_i \geq p_i \\ f_i & q_i \leq f_i \leq p_i \\ q_i & f_i \leq q_i \end{cases}$, x_d, y_d and z_d are the desired displacement of the mechanism, x_r, y_{rx} and $y_{r\theta}$ are signals after compensation and they are inputted to the modified inverse P-I model, four piecewise functions D_i (i=1, 2, 3, 4) are used to calculate the decoupling compensation signal, L is the distance between the two piezoelectric actuators (PZT_2 and PZT_3) in the x direction as shown in Fig. 1(a), the parameter $\boldsymbol{\Delta k}$, $\boldsymbol{\Delta b}$, $\boldsymbol{p}$, $\boldsymbol{q}$ determined from the

experimental data are listed in Table 2, if the value of p or q is ±10, it means that particular cutoff is useless for the decoupling signal.

After the coupling compensation, the final voltage u'_{in} inputted into the piezoelectric can be obtained by following equation.

$$u'_{in} = \Gamma^{-1}\left(y_r, \dot{y}_r\right) + \left(k_p e(t) + k_i \int_0^t e(\tau) d_\tau\right) \tag{12}$$

where y_r is the signal after compensation.

Table 2. Parameter of decoupling algorithm

i	Δk_i	Δb_i	p_i	q_i
1	0.38	-0.38	2.05	10
2	0.31	-0.70	10	-10
3	-0.20	1.50	0.27	-10
4	-0.75×10^{-2}	0.87	10	-0.18

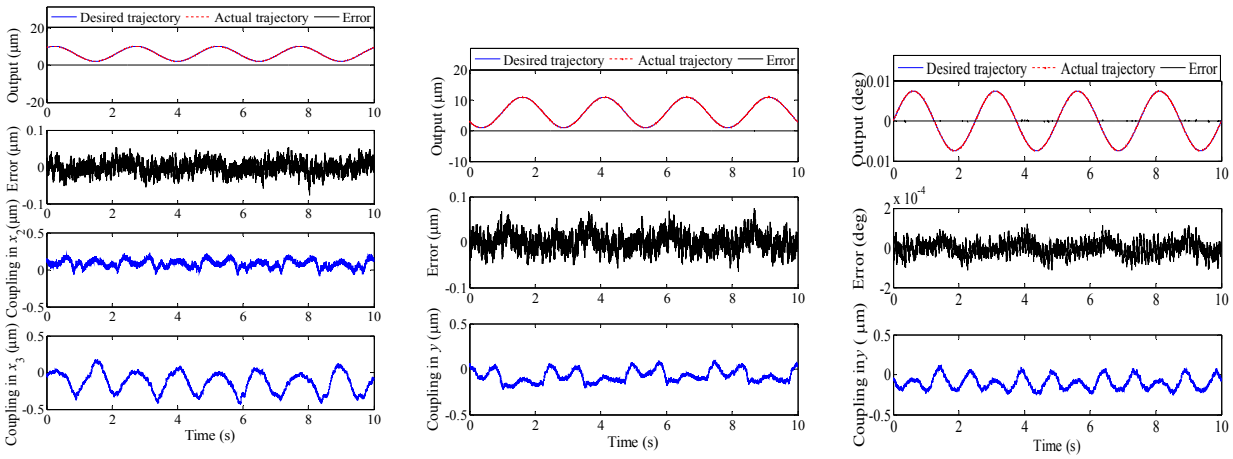

(a) (b) (c)

Fig. 10. The trajectory tracking of a sinusoidal signal and coupling error with decoupling feedforward/feedback controller: (a) trajectory tracking in the y direction and coupling error in x_2 and x_3; (b) trajectory tracking in the x direction and coupling error in y; (c) trajectory tracking in the θ_Z direction and coupling error in y.

5. Trajectory tracking testing

In order to examine the decoupling performance of the fully developed control methodology, a 1-D trajectory is firstly utilized. Single axis sinusoidal trajectory tracking under the same experimental conditions as the previous tracking tests are implemented, allowing easy comparison to the results in Fig. 7. Fig. 10 shows the desired and actually obtained trajectories as well as the associated tracking errors and coupling errors. The platform follows the desired trajectory with tracking errors very similar to those seen in the previous experiments. However, the coupling motion have been significantly reduced. Details of the decoupling performance are summarized in

Table 3. Compared with the controller lacking decoupling compensation, the spans of the coupling error ranges have been reduced by a factor of 3.8-7.0 times. These demonstrate the effectiveness of the proposed decoupling feedforward/feedback controller. What's more, considering the rate-dependence of the hysteresis, a new composed signal with multi frequencies as listed in Eq. 13 is tracked and the results are shown in Fig. 11, the maximal and RMS tracking error are 0.1466 μm and 0.0425 μm, respectively, pointing out the effectiveness of the proposed hysteresis model and the constructed controller.

$$u = 5.5 + 1.5\sin(2\pi t - 0.5\pi) + \sin(0.6\pi t - 0.5\pi) + \sin(\pi t - 0.5\pi) \tag{13}$$

The 3-DOF flexure-based mechanism is intended for planar motion and so further insights on the performance of the decoupling controller were sought through 2-D trajectory tracking tests. A circular trajectory in the *xy* plane with radius of 5 μm was examined using the new

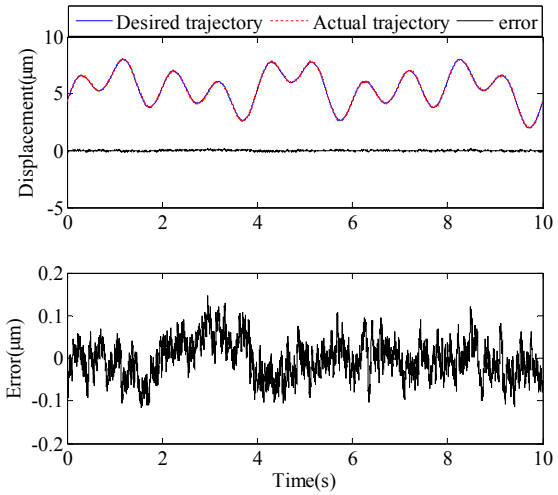

Fig. 11. The trajectory tracking of a new composed signal

Table 3. The range and span of the coupling error with and without decoupling algorithm

		Coupling error with feedforward/feedback controller (μm)	Coupling error with decoupling feedforward/feedback controller (μm)
Coupling error in x_2 from y	Range	[0.4272, 2.6337]	[-0.0846, 0.2327]
	Span	2.2065	0.3173
Coupling error in x_3 from y	Range	[0.1740, 2.9175]	[-0.4380, 0.1772]
	Span	2.7435	0.6152
Coupling error in y from x	Range	[-0.7874, 0.4608]	[-0.2246, 0.0993]
	Span	1.2482	0.3239
Coupling error in y from rotation	Range	[-0.2258, 1.4526]	[-0.2535, 0.1183]
	span	1.6784	0.3718

feedforward/feedback controller with and without enabling the decoupling algorithm. The signal input into the x and y directions are respectively as follows:

$$x = 5\sin\left(0.8\pi t\right) + 6 \tag{14}$$

$$y = 5\sin\left(0.8\pi t - 0.5\pi\right) + 6 \tag{15}$$

As shown in Fig. 12, the moving platform follows the demand trajectory quite well in both conditions but the tracking property is significantly improved when the decoupling technique is enabled. The 2-norm of the contouring error can be easily calculated in Matlab software and which are 11.19 and 5.72 with and without the decoupling compensation, respectively. What's more, as the tracking error curves shown, the tracking errors in the x and y directions are within ±97 nm and ±65 nm with decoupling control, but ±162 nm and ±117 nm in the x and y directions, respectively, without decoupling compensation. These demonstrate that the cross-axis coupling motion in xy plane is effectively compensated using the new control scheme.

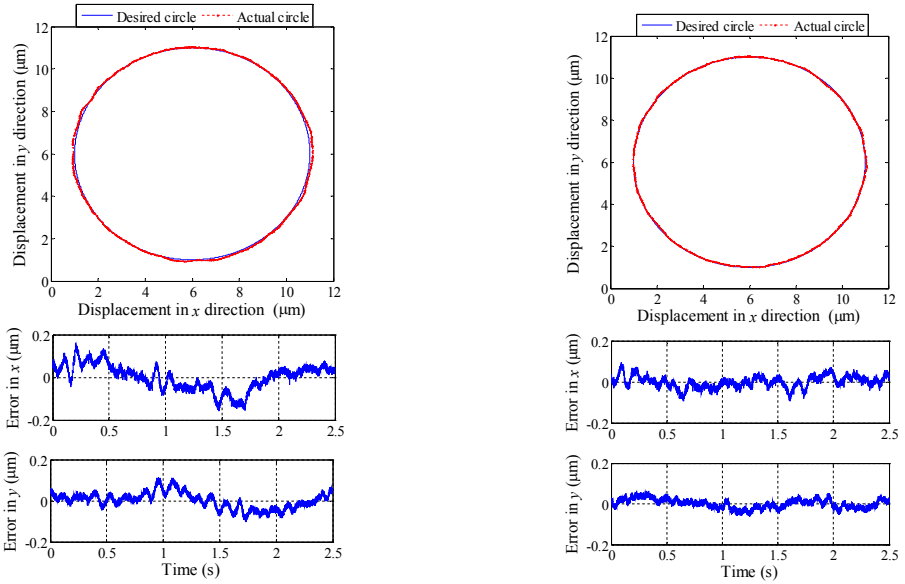

(a) (b)

Fig. 12. Tracking of a circular trajectory in the x and y directions: (a) with feedforward/feedback controller; (b) with decoupling feedforward/feedbak controller.

Since the mechanism also realizes the rotational motion to adjust the orientation of the moving platform, a good decoupling between the translational and rotational motions is also important. It was evaluated by experimental tests of the motion in the y direction and the θ_Z direction, a translation in the y direction and a rotation about the z axis were simultaneously actuated, the rotation command is given by

$$\theta_z = 9.2\sin\left(0.8\pi t\right)\times 10^{-3} \tag{16}$$

The trajectories and errors are shown in Fig. 13 with and without enabling the decoupling control algorithm. Again, the tracking accuracy is improved when decoupling is enabled; tracking errors were reduced roughly from [-1.68×10-4, 1.87×10-4] deg to [-1.73×10-4, 1.11×10-4] deg in the θ_Z direction and from [-170, 123] nm to [-113, 102] nm in the y direction. These demonstrate the effectiveness of the developed controller for the decoupling of the rotational and translation motion.

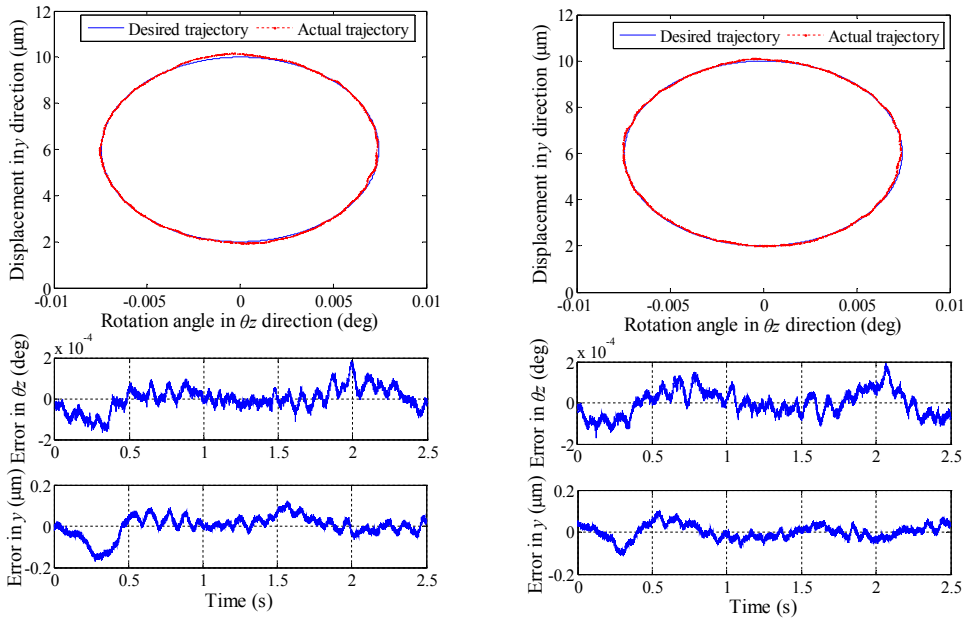

(a) (b)

Fig. 13. Tracking of a 2-D trajectory with rotation in the θ_Z direction and translation in the y directions: (a) with feedforward/feedback controller; (b) with decoupling feedforward/feedbak controller.

6. Conclusions

A modified inverse P-I hysteresis model including backlash operators, dead-zone operators and a cubic polynomial function has been established. The thresholds of backlash operators and dead-zone operators have been optimized and the rate-dependent phenomenon has been modeled using linearly weighted variation method. The predictions of the identified inverse hysteresis model showed close agreement with experimental curves. The model is incorporated in the feedforward controller for a planar 3-DOF flexure mechanism intended for micrometer-scale operations. A feedforward/feedback controller has then been proposed to reduce the effects of external disturbances and improve the static and dynamic performance of the entire system. Experimental study of tracking sinusoidal demand signals has confirmed the effectiveness of the proposed model and identification methodologies.

Because a degree of residual cross-coupling between the axis of such mechanism is inevitable in practice, a decoupling algorithm has been developed and incorporated in the feedforward/feedback controller. Under the requirement of a single axis motion, experimental testing has verified that the error motion coupled into each axis is significantly reduced when using the new decoupling feedforward/feedback controller. Further testing by 2-D trajectory tracking showed that the decoupling feedforward/feedback controller significantly improved the trajectory tracking performance of the whole system. The new approach can be readily adapted for the decoupling control of other kinds of flexure-based mechanisms.

In order to further improve the static and dynamic characteristics including the high frequency trajectory tracking performance, our future work will focus on the laser interferometry based sensing and measurement technique to improve the robustness and stability of the proposed novel feedforward/feedback control methodology.

Acknowledgement

This research is supported by National Natural Science Foundation of China (Nos. 51275337, 51175372, 51405333), National Key Special Project of Science and Technology of China (No. 2011ZX04016-011), Reserved Academic Program of Peiyang Scholar, and Program for New Century Excellent Talents in University (No. NCET-11-0374).

References

[1] Y. Yan, Z. Hu, X. Zhao, T. Sun, “Top-down nanomechanical machining of three-dimensional nanostructures by atomic force microscopy,” Small, 6 (2010) 724-728.

[2] N. Bonnail. “Variable structure of a piezoelectric actuator for a scanning tunneling microscope,” IEEE Transaction on Industrial Eletronics, 51 (2004) 354-363.

[3] S. Thalhammer, “Laser micro-tools in cell biology and molecular medicine,” Laser Physics, 13 (2003) 681-691,.

[4] H.-S. Lee, J.-Y. Park, S.-M. Cha, “Ribbon plastic optical fiber linked optical transmitter and receiver modules featuring a high alignment tolerance,” Optics Express, 19 (2011) 4301-4309.

[5] Y. Zheng, P. Li, N. Zhao, “Kinetics of molecular transitions with dynamic disorder in single-molecule pulling experiments,” The Journal of Chemical Physics, 138 (2013) 204102.

[6] T. Zeng, K. L. cooper etc, “Molecularly self-assembled actuators and devices,” Smart Structures and Materials 2001: Electroactive Polymer Actuatos and Deveces, Newport Beach, CA: Society of Photo-Optical Instrumentation Engineers, 4329 (2001).

[7] B. A. Gozen, O. B. Ozdoganlar, “Design and evaluation of a mechanical nanomanufacturing system for nanomilling,” Precision Engineering, 36 (2012) 19-30.

[8] Y. Tian, D. Zhang, B. Shirinzadeh, “Dynamic modeling of a flexure-based mechanism for ultra-precision grinding operation,” Precision Engineering, 35 (2011) 554-565.

[9] Y. Qin, B. Shirinzadeh, D. Zhang, Y. Tian, “Design and Kinematics Modeling of a Novel 3-DOF Monolithic Manipulator Featuring Improved Scott-Russell Mechanisms,” Journal of Mechanical Design, 135 (2013) 101004.

[10] Y. Tian, Z. Guo, F. Wang, J. Li, D. Zhang, B. Shirinzadeh, “Design and experimental investigation of a 2-DOF planar micro-positioning table,” International Journal of Intelligent Mechatronics and Robotics (IJIMR), 3 (2013) 39-54.

[11] Y. K. Yong, S. S. Aphale, and S. O. R. Moheimani, “Design, Identification, and Control of a Flexure-Based XYStage for Fast Nanoscale Positioning,” IEEE Transactions on nanotechnology, 8 (2009) 46-54.

[12] T. J. Teo, G. Yang and I.-M. Chen, "A Large Deflection and High Payload Flexure-Based Parallel Manipulator for UV Nanoimprint Lithography - Part I. Modeling and Analyses", Precision Engineering, 38 (2014) 861-871.

[13] G. Z. Lum, T. J. Teo, G. Yang, S. H. Yeo and M. Sitti, "Integrating mechanism synthesis and topological optimization technique for stiffness-oriented design of a three degrees-of-freedom flexure-based parallel mechanism", Precision Engineering, 39 (2015) 125-133.

[14] Q. Xu, “Design and development of a compact flexure-based precision positioning system with centimeter range,” IEEE Transactions on Industrial electronics, 61 (2014) 893-903.

[15] G. Gu and L. Zhu and C. Su, etc, "Modeling and control of piezo-actuated nanopositioning stages: A survey," IEEE Transaction on Automation Science and Engineering, DOI: 10.1109/TASE.2014.2352364.

[16] Y. Cao, X. B. Chen, "A survey of modeling and control issues foe piezo-electric actuators," Journal of Dynamic Systems, Measurement, and Control, 137 (2015) 014001.

[17] G. Gu and L. Zhu and C. Su, etc, "Motion control of piezoelectric positioning stages: modeling, controller design and experimental evaluation," IEEE/ASME Transactions on Mechatronics, 18 (2013) 1459-1471.

[18] L. Liu, K. K. Tan, S.-L. Chen, S. Huang, and T. H. Lee, "SVD-based Preisach hysteresis identification and composite control of piezo actuators". ISA Transactions, 51 (2012) 430-438.

[19] L. Liu, K. K. Tan, S.-L. Chen, C. S. Teo,T. H. Lee, "Discrete Composite Control of Piezoelectric Actuators for High-Speed and Precision Scanning", IEEE Transactions on Industrial Informatics, 9 (2013) 859-868.

[20] Y. Guo, J. Mao, K. Zhou, “Modeling and Control of Giant Magnetostrictive Actuator Based on Bouc-Wen Model,” Proceedings of 2011 8th Asian Control Conference (ASCC), (2011) 530-534.

[21] Y. Li and Q. Xu, “Adaptive sliding mode control with perturbation estimation and PID sliding surface for motion tracking of a piezo-driven micromanipulator,” IEEE Trans. Control Syst. Technol. 18 (2010) 798–810.

[22] W. T. Ang, P. K. Khosla, and C. N. Riviere, “Feedforward controller with Inverse rate-dependent model for piezoelectric actuators in trajectorytracking applications,” IEEE/ASME Trans. Mechatronics, 12 (2007) 134–142.

[23] M. Janaideh, S. Rakheja, C. Su, “A generalized Prandtl–Ishlinskii model for characterizing the hysteresis and saturation nonlinearities of smart actuators,” Smart Materials and Structures, 18 (2009) 045001.

[24] Y. Li, J. Huang, and H. Tang, “A compliant parallel XY micro motion stage with complete kinematic decoupling,” IEEE Transactions on Automation Science and Engineering, 9 (2012) 538-553.

[25] Y. Li, and Q. Xu, “Design and Analysis of a Totally Decoupled Flexure-Based XY Parallel Micromanipulator", IEEE Transactions on Robotics, 25 (2009) 645-657.

[26] L. Lai, G. Gu, and L. Zhu, “Design and control of a decoupled two degree of freedom translational parallel micro-positioning stage,” Review of Scientific Instruments, 83 (2012) 045105.

[27] Y. Tian, B. Shirinzadeh, D. Zhang, “Design and dynamics of a 3-DOF flexure-based parallel mechanism for micro/nano manipulation,” Microelectronic Engineering, 87 (2010) 230-241.

[28] H. Kim, D. H. Ahn and D. G. Gweon, “Development of a novel 3-degrees of freedom flexure based positioning system,” Review of Scientific Instruments, 83 (2012) 055114.

[29] H. Kim and D. Gweon, “Development of a compact and long range XYθz nano-positioning stage”, Review of Scientific Instruments, 83 (2012) 085102.

[30] Y. Qin, Y. Tian, D. Zhang, B. Shirinzadeh, “A Novel Direct Inverse Modeling Approach for Hysteresis Compensation of Piezoelectric Actuator in Feedforward Applications,” IEEE/ASME Transactions of Mechatronics, 18 (2013) 981-989.

[31] Z. Guo, Y. Tian and X. Liu, “Design and control methodology of a 3-DOF flexure-based mechanism for micro/nano positioning”, Robotics and Computer-Integrated Manufacturing, 32 (2015) 93-105.

[32] G. Gu and L. Zhu and C. Su, “Modeling and compensation of asymmetric hysteresis nonlinearity for piezoceramic actuators with a modified Prandtl-Ishlinskii model”, IEEE Transactions on Industrial Electronics, 61(2014) 1583-1595.